Mesoscopic conductance fluctuations at subdiffusion scales

V. V. Marinyuk and D. B. Rogozkin

Moscow Engineering Physics Institute (National Research Nuclear University), Kashirskoe Shosse 31, 115409, Moscow, Russia

(Received 18 February 2013; revised manuscript received 23 September 2014; published 13 March 2015)

We study the conductance fluctuations in the crossover between ballistic and diffusive regimes of phase coherent transport. Within a diagrammatic approach, the conductance variance for a quasi-one-dimensional disordered system is calculated beyond the diffusion approximation. The result obtained establishes the interrelation between conductance fluctuations in the crossover regime and the inhomogeneity characteristics of the disordered system. In the case of highly forward scattering by large inhomogeneities, we find the enhancement of conductance fluctuations at subdiffusion length scales.

DOI: 10.1103/PhysRevB.91.125125 PACS number(s): 73.23.−b, 42.25.Dd, 42.25.Hz

I. INTRODUCTION

One of the most striking phenomenon accompanying phase coherent transport in disordered systems is the "universal" conductance fluctuations (UCF) [1]. The variance of the dimensionless conductance proves to be of the order of unity and, under certain conditions [2], does not depend on the sample size. The UCF phenomenon pertains equally to both quantum electronic transport [1] and propagation of light [3] or microwaves [4] through a random medium. In the latter case, UCF have been observed in sample-specific fluctuations of speckle patterns [3,4].

Previous studies of mesoscopic conductance fluctuations (see, e.g., Refs. [2,5–14]) were mostly focused on the diffusive regime of wave transport where the length L of the sample is much larger than transport mean-free path $l_{\rm tr}$. In this regime, the effect of UCF is observed. Not much is known as regards the crossover from the ballistic to diffusive regime and, correspondingly, the fluctuations at subdiffusion length scales, $L \leqslant l_{\rm tr}$. At the same time, the effects originating from the specific features of disorder are expected to reveal themselves just in the crossover regime. This is suggested, in particular, by the recent results of numerical modeling of the conductance fluctuations in disordered graphene [15,16] where the enhanced fluctuations and their sensitivity to the spatial correlations of disorder were found. The currently available results concerned with the crossover regime are based only on direct numerical modeling [15–20], and any theoretical treatment has not been done yet. The calculations of the conductance variance with the random matrix theory (RMT) presented in Refs. [21–24] rest on the isotropy hypothesis [25] where the mean-free path l is the only characteristic of disorder and therefore do not enable one to describe the dependence of the crossover regime on the specific features of disorder.

In this paper we present an analytical result for the conductance variance of a quasi-one-dimensional (quasi-1D) system (a waveguide with bulk disorder). The diagrammatic calculations are carried out without resorting to the diffusion approximation. The variance is expressed explicitly in terms of the cross section of scattering by inhomogeneities of the medium and the propagators that obey the conventional transport equation. In the large-length limit, our result transforms with no divergencies to the well-known diffusion formula [5,8]. The crossover between the quasiballistic and diffusive regimes is studied for systems with point-like and large (as compared to wavelength λ) inhomogeneities. In the first case, our calculations within the two-stream version of the discrete-ordinate method are shown to be coincident with the RMT results [6,10,21–24]. These results, as follow from the direct calculations in the quasiballistic limit $L \leqslant l$, have a logarithmic accuracy at relatively small L and become qualitatively inapplicable as the size of inhomogeneities increases. For the system with large inhomogeneities, we find that the conductance variance in the crossover regime reaches its maximum, which can exceed the UCF value.

II. DIAGRAMMATIC CALCULATIONS

We consider transmission of monochromatic waves through a disordered waveguide of length L. The dimensionless conductance (or transmittance) of the waveguide can be defined as the sum of transmission coefficients T_{ab} connecting incoming and outgoing modes a and b, respectively (see, e.g., Refs. [5–8,10]),

$$G = \sum_{a,b} T_{ab}. \tag{1}$$

The transmission coefficients T_{ab} depend on spatial configuration of the scattering centers and vary from sample to sample.

Under conditions of weak localization ($G \gg 1$), the value of $\langle G \rangle$ averaged over an ensemble of disordered samples is governed by the so-called diffuson which, within the standard impurity technique, is the sum of ladder diagrams. The variance of conductance $\langle (\delta G)^2 \rangle$ can be expressed in terms of the ensemble-average fourth moment of a wave field and represented as expansion in orders of interference between ladders. Each interference event between the ladders contains the Hikami vertex [26]. The variance of conductance fluctuations is governed by diagrams containing two vertices (see Fig. 1). In the presence of time-reversal symmetry, the diagrams shown explicitly in Fig. 1 should be supplemented by those that are obtained by interchanging initial i and final f states in one pair of conjugated wave fields. These diagrams correspond to the time-reversed paths of wave propagation and contain the maximally crossed internal graphs (or cooperons) instead of the ladders (or diffusons).

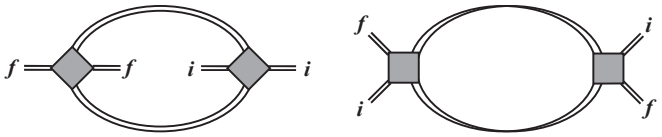

FIG. 1. Diagrams contributing to conductance variance. The paired lines correspond to diffusons. The shaded boxes are the Hikami vertices [26].

For great number N of propagating modes [$N = k_0^2 A/(4\pi)$, where k_0 is the wave number and A is the area of the waveguide cross section], the summation over modes can be replaced by integration over directions $\mathbf{\Omega}$ of wave propagation (see, e.g., Ref. [8]),

$$\sum_a \cdots = \int \frac{A d\mathbf{q}_a}{(2\pi)^2} \cdots = \frac{k_0^2 A}{(2\pi)^2} \int d\mathbf{\Omega}_a |\mu_a| \cdots , \quad (2)$$

where $\mathbf{q}_a$ is the transverse momentum ($q_a < k_0$), $\mu_a = \Omega_{az}$, and the z axis is directed along the waveguide. Hemispheres $\Omega_{az} > 0$ and $\Omega_{az} < 0$ correspond to the waves that propagate in the forward and backward directions, respectively. The average conductance is expressed in terms of the average transmission coefficient $\langle T_{ab} \rangle$ which is equal to (see Appendix A)

$$\langle T_{ab} \rangle = \frac{(2\pi)^2}{k_0^2 A} I_{ab}(z_f = L | z_i = 0), \quad (3)$$

where propagator $I_{ab}(z|z') = I(z, \mathbf{\Omega}_a | z', \mathbf{\Omega}_b)$ denotes the intensity at depth z in direction $\mathbf{\Omega}_a$ from a source placed at depth z' and emitting waves in direction $\mathbf{\Omega}_b$. Intensity I_{ab} is subject to the transport equation [27]

$$\left(\mu_a \frac{\partial}{\partial z} + n\sigma_{\text{tot}} \right) I_{ab}(z|z') = \delta(z - z') \delta(\mathbf{\Omega}_a - \mathbf{\Omega}_b) + \int d\mathbf{\Omega}_c \sigma_{ac} I_{cb}(z|z'), \quad (4)$$

where $\sigma_{ac} = n d\sigma(\mathbf{\Omega}_a \mathbf{\Omega}_c)/d\Omega$, n is the number of scattering centers per unit volume, $d\sigma/d\Omega$ is the differential scattering cross section, $\sigma_{\text{tot}} = \sigma + \sigma_{\text{a}}$ is the total cross section of interaction, and σ and σ_{a} are the cross sections of elastic scattering and absorption, respectively. In a continuous random medium, Eq. (4) remains unchanged with the only difference being that σ_{ac} means the differential scattering coefficient which is expressed via the correlation function of disorder.

The diagrams shown in Fig. 1 can be evaluated in a straightforward manner (see Appendix B). In what follows, we take into account the ladders incorporating an arbitrary number of scattering events; among them the graphs without any scattering. These latter describe nonscattered waves. Contrary to calculations performed within the diffusion approximation [5,8], we need not introduce particular diagrams containing only one internal ladder propagator and the six-point Hikami vertex. Such diagrams are already contained among the diagrams depicted in Fig. 1. They correspond to the pair of nonscattered waves in either of two internal ladders.

Our diagrammatic calculations are similar to those of Ref. [28], where the contribution from the Hikami vertex with four attached ladders was found without the diffusion approximation. The result [28] is based on the coordinate-direction representation for the Hikami vertex and the transport equation for the ladder propagators. Extending the method [28] to the case of the waveguide geometry, we derive the following expression for the conductance variance (see Appendix B):

$$\begin{aligned}\langle (\delta G)^2 \rangle = {} & \iint_0^L dz dz' \iiiint d\mathbf{\Omega}_a d\mathbf{\Omega}_b d\mathbf{\Omega}_c d\mathbf{\Omega}_d \sigma_{ab} \sigma_{cd} \\ & \times \Big\{ \left(I_a^f - I_b^f\right)^2 I_{ac} I_{bd} \left(I_c^i - I_d^i\right)^2 + \left(I_a^f - I_b^f\right)\left(I_{-a}^i - I_{-b}^i\right) I_{ac} I_{bd} \left(I_{-c}^f - I_{-d}^f\right)\left(I_c^i - I_d^i\right) \\ & + \left[\left(I_a^f - I_b^f\right) I_b^i + I_{-b}^f \left(I_{-a}^i - I_{-b}^i\right)\right](I_{ac} - I_{ad})(I_{-a-c} - I_{-b-c}) \left[\left(I_c^f - I_d^f\right) I_d^i + I_{-d}^f \left(I_{-c}^i - I_{-d}^i\right)\right] \Big\} \\ & + \int_0^L dz \iint d\mathbf{\Omega}_a d\mathbf{\Omega}_b \sigma_{ab} \left[\left(I_a^f - I_b^f\right) I_b^i + I_{-b}^f \left(I_{-a}^i - I_{-b}^i\right)\right]^2 I_{ab}(z|z), \end{aligned} \quad (5)$$

where internal propagators $I_{ab} = I_{ab}(z|z')$ obey Eq. (4), and the incoming and outgoing propagators are defined as

$$I_a^i(z) = \int d\mathbf{\Omega}_b |\mu_b| I_{ab}(z|z_i = 0), \quad (6)$$

$$I_a^f(z) = \int d\mathbf{\Omega}_b |\mu_b| I_{ba}(z_f = L|z). \quad (7)$$

The change of sign in a subscript of any propagator entering into Eq. (5) implies reversing the direction (i.e., substitution of $-\mathbf{\Omega}_a$ for $\mathbf{\Omega}_a$ into the propagator). The incoming and outgoing propagators appearing in Eq. (5) with subscripts $\pm a$, $\pm b$ are functions of z, while those with subscripts $\pm c$, $\pm d$ are functions of z'.

The terms that contain products of the incoming and outgoing propagators with subscripts of opposite sign [e.g., $[(I_a^f - I_b^f) I_b^i][\cdots][I_{-d}^f (I_{-c}^i - I_{-d}^i)]$] correspond to the cooperon contribution. The cooperon contribution includes the maximally crossed internal graphs and, in the low-order-scattering limit, the internal graphs that describe the waves propagating in opposite directions [see Appendix B, e.g., Eq. (B15)]. All these diagrams generate the products of the scattering amplitudes of the form $f_{ab} f_{-b-a}$, i.e., the amplitudes of the direct and time-reversed processes. Equation (5) has the presented form provided that time-reversal symmetry is not violated.

Expressions similar to Eqs. (1), (3), and (5) are also valid for the reflection geometry. The average reflection coefficient $\langle R_{ab} \rangle$ and the reflectance variance $\langle (\delta R)^2 \rangle$ differ from Eqs. (3)

and (5) only by substitution of $z_f = 0$ for $z_f = L$ in all outgoing propagators.

Equation (5) is the principal result of our work. This equation generalizes the result of the diffusion approximation [5,8], much as the transport equation generalizes the equation of diffusion. Equation (5) establishes the interrelation between the conductance variance and the characteristics of scattering centers of the disordered system and enables us to study evolution of the fluctuations in going from the quasiballistic propagation to the diffusive regime.

Equation (5) can be extended to include the difference of the incident waves in frequency. In this case, Eq. (5) is the correlation function of conductance fluctuations of the form $\langle \delta G(\omega_0 + \Delta\omega/2)\delta G(\omega_0 - \Delta\omega/2)\rangle$. The frequency shift $\Delta\omega$ appears only in the internal propagators entering into Eq. (5). In the first two terms, the product of the internal propagators takes the form

$$I_{ac} I_{bd} = I_{ac}(\Delta\omega)\, I_{bd}(-\Delta\omega).$$

In the last two terms, the internal propagators look like

$$I_{ad} I_{-b-c} = \mathrm{Re}\{I_{ad}(\Delta\omega)\, I_{-b-c}(\Delta\omega)\},$$
$$I_{ab} = \mathrm{Re}\{I_{ab}(\Delta\omega)\}.$$

The propagator $I_{ab}(\Delta\omega) = I(z,\mathbf{\Omega}_a|z',\mathbf{\Omega}_b,\Delta\omega)$ obeys the transport equation that is obtained from Eq. (4) by substituting the complex absorption coefficient $(n\sigma_a + i\Delta\omega/c)$ for $n\sigma_a$ (c is the wave velocity).

III. DIFFUSIVE LIMIT

The results obtained previously within the diffusion approximation [5,8] can be derived from Eq. (5) by substitution of the corresponding approximate expressions for the propagators.

For a long waveguide, $L \gg l_{\mathrm{tr}}$, the main contribution to the integrals over z and z' is governed by the distances that are far away from the input and output waveguide boundaries. Therefore, low-order-scattering contributions to Eq. (5) should be neglected. In this case, the propagators turn out to depend only slightly on the directions and can be expanded in terms of the spherical harmonics. The first terms of such expansion for the internal propagator have the form

$$I_{ab} = \frac{1}{(4\pi)^2}[\Phi(z|z') + 3\mu_a J(z|z') - 3\mu_b J(z'|z) + \cdots], \tag{8}$$

where "density" Φ and "current" J are defined as

$$\Phi(z|z') = \iint d\mathbf{\Omega}_a d\mathbf{\Omega}_b I_{ab}(z|z'), \tag{9}$$

$$J(z|z') = \iint d\mathbf{\Omega}_a d\mathbf{\Omega}_b \mu_a I_{ab}(z|z'). \tag{10}$$

Analogous expansions are also valid for the incoming and outgoing propagators,

$$I_a^{i,f} = \frac{1}{4\pi}[\Phi_{i,f}(z) + 3\mu_a J_{i,f}(z) + \cdots], \tag{11}$$

where

$$\Phi_{i,f} = \int d\mathbf{\Omega}_a I_a^{i,f}, \quad J_{i,f} = \int d\mathbf{\Omega}_a \mu_a I_a^{i,f}. \tag{12}$$

Substituting these expansions into Eq. (5) and performing integration over all directions, we arrive at the diffusion formula for the conductance variance:

$$\langle(\delta G)^2\rangle = \left(\frac{3}{32\pi^3 l_{\mathrm{tr}}}\right)^2 \iint_0^L dz dz' \Big\{ J_f^2(z)\Phi^2(z|z')J_i^2(z') + J_f(z)J_i(z)\Phi^2(z|z')J_f(z')J_i(z')$$
$$+ [J_f(z)\Phi_i(z) - J_i(z)\Phi_f(z)]\left[J(z|z')J(z'|z) + \frac{2\pi l_{\mathrm{tr}}}{3}\delta(z-z')\Phi(z|z)\right][J_f(z')\Phi_i(z') - J_i(z')\Phi_f(z')]\Big\}, \tag{13}$$

where transport mean-free path l_{tr} is defined as

$$l_{\mathrm{tr}}^{-1} = \int d\mathbf{\Omega}_a (1 - \mathbf{\Omega}_a\mathbf{\Omega}_b)\sigma_{ab}. \tag{14}$$

Within the diffusion approximation (see, e.g. Ref. [27]), the current J is expressed in terms of the z derivative of the density Φ:

$$J(z|z') = -\frac{l_{\mathrm{tr}}}{3}\frac{\partial\Phi(z|z')}{\partial z}, \quad J_{i,f}(z) = \mp\frac{l_{\mathrm{tr}}}{3}\frac{\partial\Phi_{i,f}(z)}{\partial z}, \tag{15}$$

and Eq. (13) can be transformed into the same form as in Refs. [5,8]. For a waveguide with no absorption, Eq. (13) gives the well-known result [6,8,10] $\langle(\delta G)^2\rangle = 2/15$.

It should be emphasized that any divergent terms do not arise in Eq. (5) in going to the diffusive limit. As is known [5,8], the straightforward diagrammatic calculations within the diffusion approximation result in the divergent terms. To cancel them, an additional treatment is required [5,8].

IV. TWO-STREAM MODEL

As an illustration of the application of Eq. (5) to calculating the conductance variance beyond the diffusion approximation, we find $\langle(\delta G)^2\rangle$ within the two-stream version of the discrete-ordinate method [27,29]. This simplest model enables us to perform integration in Eq. (5) explicitly and to derive an analytical formula for $\langle(\delta G)^2\rangle$ which describes the crossover between the quasiballistic and diffusive regimes.

Within this approach, each integral over $\mathbf{\Omega}$ is supposed to be equal to the sum of the values of an integrand quantity at $\Omega_z = \pm\mu_0$,

$$\int d\mathbf{\Omega}_a I(z,\mathbf{\Omega}_a) = 2\pi I_+(z) + 2\pi I_-(z), \tag{16}$$

where $I_\pm(z) = I(z,\Omega_z = \pm\mu_0)$, and $\pm\mu_0$ are the discrete ordinates [27].

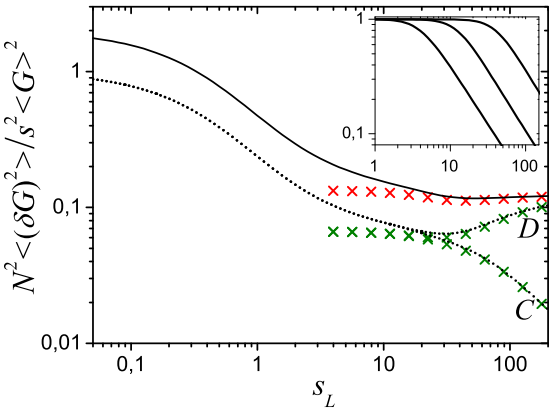

FIG. 2. (Color online) Variance of conductance fluctuations as a function of the waveguide length (absorption length $l_a = 10^3 l$). The diffuson (D) and cooperon (C) contributions to $\langle(\delta G)^2\rangle$ are shown by dotted lines. Crosses are the RMT results for the diffusive regime [10]. The inset compares the cooperon-to-diffuson ratio for different absorption lengths (from upper to lower curves, $l/l_a = 0.001$, 0.01, and 0.1).

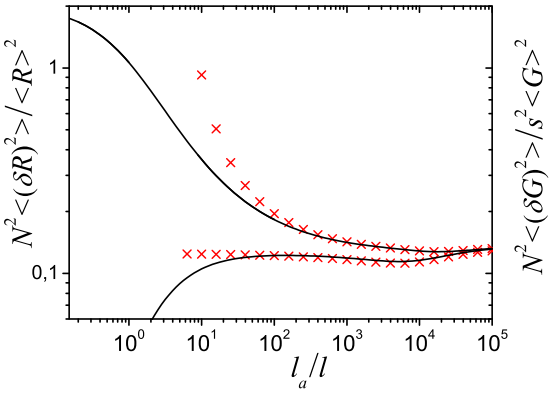

FIG. 3. (Color online) Reflectance (upper curve) and conductance (lower curve) fluctuations as functions of the absorption length. The dimensionless waveguide length $s_L = 100$. The RMT results for the diffusive regime [10] are shown by crosses.

For a widely used model of point-like centers, the quantity σ_{ab} in Eqs. (4) and (5) is independent of direction; $\sigma_{ab} = n\sigma/(4\pi)$, and the disorder is characterized only by the mean-free path $l = (n\sigma)^{-1}$. In this case, Eq. (5) is expressed in terms of the values of intensity propagators at $\pm\mu_0$ as follows:

$$\langle(\delta G)^2\rangle = \left(\frac{\pi}{l}\right)^2 \iint_0^L dz dz' \Big\{ 2(I_{++}I_{--} + I_{+-}I_{-+})[(I_+^f - I_-^f)^2 (I_+^i - I_-^i)'^2 + (I_+^f - I_-^f)(I_+^i - I_-^i)(I_+^f - I_-^f)'(I_+^i - I_-^i)'] + [h_+(I_{++} - I_{+-}) + h_-(I_{--} - I_{-+})][h'_+(I_{--} - I_{+-}) + h'_-(I_{++} - I_{-+})] \Big\} + \frac{\pi}{l}\int_0^L dz [h_+^2 I_{+-}(z|z) + h_-^2 I_{-+}(z|z)], \tag{17}$$

where

$$h_\pm = [\pm(I_+^f - I_-^f)I_\mp^i \mp (I_+^i - I_-^i)I_\pm^f],$$

and the propagators $I_{\pm\pm} = I_{\pm\pm}(z|z')$ and $I_\pm^{i,f} = I_\pm^{i,f}(z)$ entering into Eq. (17) are determined analytically from the transport equation and given in Appendix C. In Eq. (17), the incoming and outgoing propagators marked by primes are functions of z'; otherwise they are functions of z.

For a waveguide with no absorption, Eq. (17) results in

$$\langle(\delta G)^2\rangle = \frac{2}{15}\left(1 - \frac{1 + 6s_L}{(1 + s_L)^6}\right), \tag{18}$$

where $s_L = (1/2\mu_0)(L/l)$. Equation (18) coincides with the result of RMT calculations [21,23].

For purely elastic scattering, the reflectance variance coincides with the conductance variance: $\langle(\delta R)^2\rangle = \langle(\delta G)^2\rangle$. As applied to the reflection geometry, Eq. (18) gives the relation $N^2\langle(\delta R)^2\rangle/\langle R\rangle^2 = 2$ at $s_L \ll 1$. In this limit, only single-scattered waves contribute to reflectance fluctuations. The factor "two" arises from two scattering processes which differ from each other by interchanging the final and initial states. This agrees with RMT treatment [6,21,24].

Analytical formulas that extend Eq. (18) to a waveguide with absorption are too cumbersome to be presented here and, therefore, we illustrate the length dependence of the conductance variance in graphical form [see Fig. 2; absorption length l_a is defined as $l_a = (n\sigma_a)^{-1}$]. As follows from the calculations, the difference between the diffuson and cooperon contributions manifests itself at large L and increases with increasing absorption. A decrease in the cooperon contribution to conductance fluctuations results from suppression of loop trajectories [10]. In the presence of absorption, $\langle(\delta G)^2\rangle$ is no longer equal to $\langle(\delta R)^2\rangle$. While relative conductance fluctuations fall off with absorption, the relative fluctuations of reflectance increase (see Fig. 3). In the diffusive limit (large L, $L \gg l$, and weak absorption, $l_a \gg l$) our results are in agreement with analytical RMT calculations [10] for both the transmission and reflection geometries [30]. Our results coincide also with numerical integration of the RMT equations for the reflectance variance [22] (see Fig. 4).

The results obtained above could be extended to the case of anisotropic scattering by the relation

$$\int d\mathbf{\Omega}_a \sigma_{\pm,a} I(z, \mathbf{\Omega}_a) = n\sigma(pI_\pm(z) + (1-p)I_\mp(z)), \tag{19}$$

where the factor p governs the single-scattering anisotropy (for isotropic scattering $p = 1/2$, for highly forward scattering by large inhomogeneities, the factor p tends to unity: $1-p \ll 1$). In this approximation, the conductance variance $\langle(\delta G)^2\rangle$ is obtained from Eq. (18) by substitution of $l/2(1-p)$ for

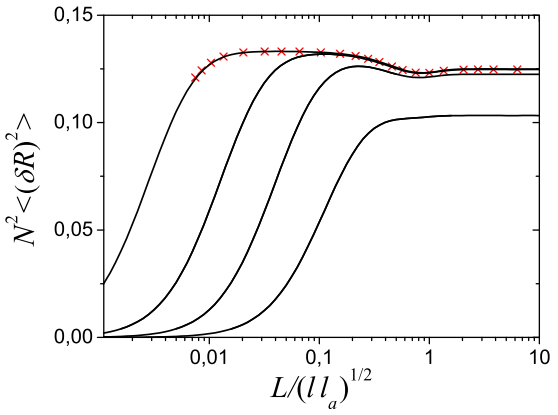

FIG. 4. (Color online) Reflectance variance as a function of the waveguide length (from upper to lower curves, the absorption length $l_a/l = 2\times10^4, 10^3, 10^2$, and 10). Crosses are the results of numerical integration of the RMT equations [22].

l. The quantity $l/2(1-p)$ is an analog of the transport mean-free path $l_{\rm tr}$. Transformation to the UCF regime occurs at $L \gg l/2(1-p)$. This qualitatively agrees with the diffusive transport condition, $L \gg l_{\rm tr}$. However, such an approach proves to be too rough to describe conductance fluctuations at subdiffusion lengths. At $L < l/2(1-p)$, it gives

$$\langle(\delta G)^2\rangle = 8\,(1-p)^2\, s_L^2. \tag{20}$$

As shown below, for isotropic scattering, Eq. (20) is applicable at $L < l$ with logarithmic accuracy. For a disordered system with large inhomogeneities, accurate calculations, contrary to Eq. (20), point out that conductance fluctuations are enhanced and not suppressed at $L < l_{\rm tr}$.

V. QUASIBALLISTIC REGIME

In transmission through a short waveguide, $L \leqslant l$, conductance variance $\langle(\delta G)^2\rangle$ can be calculated by expanding the propagators that enter into Eq. (5) in orders of wave scattering. The single-scattering contributions to $\langle(\delta G)^2\rangle$ cancel each other (see, e.g., Ref. [5]). Thus, $\langle(\delta G)^2\rangle$ is governed by the second-order scattering contributions,

$$\begin{aligned}\langle(\delta G)^2\rangle = &\int_0^L\int_0^L dz dz' \iiiint d\mathbf{\Omega}_a d\mathbf{\Omega}_b d\mathbf{\Omega}_c d\mathbf{\Omega}_d \sigma_{ab}\sigma_{cd}\\ &\times\Big\{\big(I_a^f - I_b^f\big)^2 I_{ac} I_{bd}\big(I_c^i - I_d^i\big)^2\\ &+ I_{ad} I_{-b-c}\big[I_{-b}^f I_{-b}^i I_d^f I_d^i + I_b^f I_b^i I_{-d}^f I_{-d}^i\big]\Big\}^{(0)}\\ &+\int_0^L dz \iint d\mathbf{\Omega}_a d\mathbf{\Omega}_b\Big\{\big(I_b^f I_b^i\big)^2 + \big(I_a^f I_a^i\big)^2\Big\}^{(0)}\\ &\times\sigma_{ab} I_{ab}^{(1)}(z|z),\end{aligned} \tag{21}$$

where $\{I\cdots I\}^{(0)} = I^{(0)}\cdots I^{(0)}$, $I^{(0)}$ is the nonscattered intensity, and $I^{(1)}$ is the single-scattered intensity [see Appendix A, Eq. (A11) and the text below it]. For the reflection geometry, a similar expansion in Eq. (5) gives the more compact result

$$\begin{aligned}\langle(\delta R)^2\rangle = &\int_0^L dz \iint d\mathbf{\Omega}_a d\mathbf{\Omega}_b \sigma_{ab}\\ &\times\Big\{\big(I_a^f I_b^i + I_{-b}^f I_{-a}^i\big)^2\Big\}^{(0)} I_{ab}^{(1)}(z|z).\end{aligned} \tag{22}$$

Substituting the explicit expressions for $I^{(0)}$ and $I^{(1)}$ into Eqs. (21) or (22) we arrive at the results below.

In the case of the above-mentioned model of point-like centers, we have at $L \ll l$

$$\langle(\delta G)^2\rangle = \big\langle(\delta R)^2\big\rangle = \frac{1}{2}\left(\frac{L}{l}\right)^2 \ln^2\frac{l}{L}. \tag{23}$$

This result is a counterpart of Eq. (20) at $p = 1/2$. Thus, Eq. (23) indicates a logarithmical accuracy of the two-stream approximation and, correspondingly, the RMT calculations at subdiffusion lengths.

A striking effect arises in wave transport through a system with large (as compared with wavelength λ) inhomogeneities. To model the differential cross section of scattering by large inhomogeneities we take advantage of Gaussian parametrization:

$$\frac{d\sigma}{d\Omega}(\vartheta) = \frac{\sigma}{\pi\vartheta_0^2}\exp\left[-4\sin^2(\vartheta/2)/\vartheta_0^2\right], \tag{24}$$

and a power-law parametrization:

$$\frac{d\sigma}{d\Omega}(\vartheta) = \sigma\frac{(\alpha-2)\,\vartheta_0^{\alpha-2}}{2\pi\left[\vartheta_0^2 + 4\sin^2(\vartheta/2)\right]^{\alpha/2}}, \tag{25}$$

where $\vartheta_0 = 1/(k_0 a)$ is the characteristic angle of single scattering by an inhomogeneity of size a. For large inhomogeneities, angle $\vartheta_0 \ll 1$ and the highly forward scattering dominates.

The first model can be thought as corresponding to Gaussian correlations between inhomogeneities of a refractive index (or of a random potential in the case of electronic transport).

The power-law cross section unifies numerous models of scattering. For $\alpha = 4$, Eq. (25) describes scattering of waves by weakly refracting discrete inhomogeneities of a given radius [31] as well as by a continuous medium with the Booker–Gordon correlation function [27]. For $\alpha = 3$, Eq. (25) coincides with the Henyey–Greenstein cross section, which is used very widely to model scattering of waves in random media [27]. Parametrization (25) corresponds also to the model of scattering by a fractal [32,33] with the spatial correlation function of the form $(r/a)^{(\alpha-3)/2}K_{(\alpha-3)/2}(r/a)$, where $K_\nu(x)$ denotes the modified Bessel function of second kind, a is the disorder correlation distance. Exponent α is related to the fractal dimension [32,33].

From Eq. (21) it follows that the second-order scattering contribution to the conductance variance, excluding factor $1/\vartheta_0$, proves to be a universal function of ratio $L/(l\vartheta_0)$ in the limit $\vartheta_0 \ll 1$. For the different models of scattering the corresponding dependence is illustrated in Fig. 5. With increasing L the conductance variance first increases as

$$\big\langle(\delta G)^2\big\rangle \sim (1/\vartheta_0)\,(L/l\vartheta_0)^2\ln^2(L/l\vartheta_0), \tag{26}$$

and then peaks at $L \sim 0.25 l\vartheta_0$. For rather small ϑ_0, the peak value of the conductance variance can exceed the UCF value (see the inset in Fig. 5).

VI. FLUCTUATIONS IN A SYSTEM WITH LARGE INHOMOGENEITIES

According to Eq. (1) a decrease in conductance G with increasing L and an appearance of conductance fluctuations

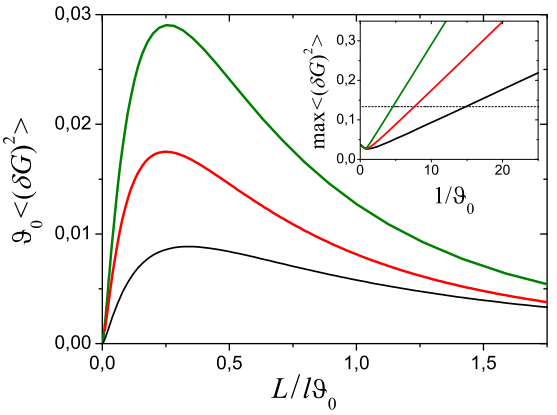

FIG. 5. (Color online) Conductance variance within the second-order-scattering approximation as a function of the waveguide length (from upper to lower curves, the Gaussian and power law, $\alpha = 4$ and $\alpha = 3$, models). The inset shows the peak value of the conductance variance as a function of parameter $1/\vartheta_0$. The horizontal dotted line is the UCF value. In the limit of point-like centers, $k_0 a \to 0$, the curves converge to a single point.

are due to the wave trajectories reflected from the sample (there are no fluctuations without reflection). For a relatively short waveguide, $L < l_{\rm tr}$, multiple wave scattering occurs predominantly through small angles. Therefore, only the waves incoming nearly parallel to the input cross section of the sample (i.e., the highest modes) can be reflected from it. These are just the waves which contribute to the variance of conductance fluctuations. Such an idea was previously used to explain [34] the destruction of conductance quantization in the quasiballistic transport of electrons through quantum wires.

Mathematically, a distinctive role of the trajectories that are nearly parallel to the input (or output) cross section of the sample follows directly from Eq. (5). Quantity $\sigma_{ab}(I_a - I_b)$ entering into Eq. (5) differs from zero only for directions $|\Omega_{az}|, |\Omega_{bz}| \ll 1$.

For $L < l_{\rm tr}$ we can find propagators entering into Eq. (5) within the small-angle approximation, putting $\Omega_{az} = \sin\zeta_a \approx \zeta_a \ll 1$. Then the transport equation (4) for a waveguide with no absorbtion can be presented in the following form [35]:

$$\zeta_a \frac{\partial}{\partial z} I_{ab} = \delta(z - z')\delta(\zeta_a - \zeta_b)\,\delta(\varphi_a - \varphi_b) + \frac{(\alpha - 2)\,\vartheta_0^{\alpha-2}}{2\pi l} \times \iint_{-\infty}^{\infty} \frac{d\zeta_c d\varphi_c\,(I_{cb} - I_{ab})}{\left[\vartheta_0^2 + (\zeta_c - \zeta_a)^2 + (\varphi_c - \varphi_a)^2\right]^{\alpha/2}}, \tag{27}$$

where the differential cross section (25) is used, and φ_a is the azimuth of direction $\mathbf{\Omega}_a$. A solution to Eq. (27) is expressed in terms of a function of dimensionless variables and parameter $L/l\vartheta_0$:

$$I_{ab}(z|z') = \frac{1}{\vartheta_0^3} f\left(\frac{\zeta_a}{\vartheta_0}, \frac{z}{L}, \frac{\zeta_b}{\vartheta_0}, \frac{z'}{L}, \frac{\varphi_a - \varphi_b}{\vartheta_0}; \frac{L}{l\vartheta_0}\right). \tag{28}$$

The fact that propagator I_{ab} within the small-angle approximation can be presented in the form of Eq. (28) enables us to draw a conclusion regarding the length dependence of variance $\langle(\delta G)^2\rangle$. Substituting Eq. (28) into the general formula for $\langle(\delta G)^2\rangle$ [see Eq. (5)], we arrive at the following equation:

$$\langle(\delta G)^2\rangle = \frac{1}{\vartheta_0} F_\alpha\left(\frac{L}{l\vartheta_0}\right), \tag{29}$$

where $F_\alpha(x)$ is a function of dimensionless parameter $L/l\vartheta_0$. The form of function $F_\alpha(x)$ is governed only by exponent α appearing in the angular dependence of the differential cross section. The x dependence of this function is given by

$$F_\alpha(x) \sim \begin{cases} x^2 \ln^2(1/x), & x \ll 1 \\ x^{-1/(\alpha-1)}, & x \gg 1, \end{cases} \tag{30}$$

and can be obtained as described below.

For rather small values of the waveguide length, $x = L/l\vartheta_0 \ll 1$, the variance of conductance fluctuations $\langle(\delta G)^2\rangle$ can be calculated within the second-order-scattering approximation [see Eq. (26)]. Comparing the result of calculations with Eq. (29), we find $F_\alpha(x)$ at $x \ll 1$.

For rather great values $x = L/l\vartheta_0 \gg 1$, wave propagation in the sample presents multiple scattering through small angles. In this case the characteristic angular spread of multiply scattered waves exceeds essentially the single-scattering angle ϑ_0. Therefore, quantity ϑ_0 can be neglected in the denominator of the differential cross section entering into the collision integral of the transport equation (27). For $\alpha < 4$, no divergency appears in Eq. (27) because the singularity in the denominator at $\zeta_c = \zeta_a$ and $\varphi_c = \varphi_a$ is canceled from the difference $I_{cb} - I_{ab}$ in the numerator [35]. Within this approximation a solution to the transport equation can be presented in the self-similar form as a function of dimensionless variables

$$I_{ab}(z|z') = \frac{1}{\zeta_L^3} \tilde{f}\left(\frac{\zeta_a}{\zeta_L}, \frac{z}{L}, \frac{\zeta_b}{\zeta_L}, \frac{z'}{L}, \frac{\varphi_a - \varphi_b}{\zeta_L}\right), \tag{31}$$

where

$$\zeta_L = (L/l_{\rm tr})^{1/(\alpha-1)} \tag{32}$$

is the characteristic multiple-scattering angle for the sample of length L, the transport mean-free path is equal to $l_{\rm tr} = c_\alpha l/\vartheta_0^{\alpha-2}$, and $c_\alpha = 2^{\alpha-3}(4-\alpha)/(\alpha-2)$.

The origin of ζ_L can be clarified as follows: Consider a wave incident on the sample at angle ζ. For a power-law differential cross section with $2 < \alpha < 4$ the angular spread of multiply scattered waves that is gained over path L/ζ can be estimated as [27,33,36] $(L/\zeta l_{\rm tr})^{1/(\alpha-2)}$. Wave reflection occurs only if the angular spread of waves is of order or exceeds the angle of incidence ζ. From condition $(L/\zeta l_{\rm tr})^{1/(\alpha-2)} \sim \zeta$ we find the characteristic angle $\zeta_L = (L/l_{\rm tr})^{1/(\alpha-1)}$. Physically, angle ζ_L separates the transmission through the sample from the reflection by it. The waves are mainly reflected from the sample and the total reflection coefficient tends to unity if the angle of incidence on the sample is less than ζ_L; otherwise, $\zeta > \zeta_L$, the waves are transmitted through the sample.

Substitution of the propagators in the form of Eq. (31) into Eq. (5) results in the following relation:

$$\langle(\delta G)^2\rangle \sim \frac{1}{\zeta_L}. \tag{33}$$

Comparison of Eqs. (33) and (32) with Eq. (29) gives the asymptotic formula for function $F_\alpha(x)$ at $x \gg 1$.

Equation (32) is applicable provided that $2 < \alpha < 4$. For $\alpha = 4$, this result has a logarithmic accuracy. In the case of the differential cross sections decreasing with angle ϑ more rapidly (by the power law with $\alpha > 4$ or by the Gaussian law), Eq. (32) is generalized as follows: For $\alpha > 4$, the characteristic angle ϑ_0 appearing in Eq. (27) cannot be neglected in the denominator. Instead of that, the propagator I_{cb} can be expanded in angles of single-scattering deflection $\zeta_c - \zeta_a$ and $\varphi_c - \varphi_a$, resulting in the Fokker–Planck approximation in Eq. (27) [35–37]. Then, in going to dimensionless variables, we obtain ζ_L in the form of Eq. (32), with the only difference being that the exponent α should be $\alpha = 4$. So, for rapidly decreasing cross sections, the multiple-scattering angle ζ_L takes the universal form [37] $\zeta_L = (L/l_{\rm tr})^{1/3}$.

According to Eqs. (29) and (30), the variance of the conductance fluctuations is inversely proportional to the single-scattering angle ϑ_0 for short samples, $L < l\vartheta_0$ or to the multiple-scattering angle ζ_L for the samples of length $l\vartheta_0 < L < l_{\rm tr}$. The appearance of these factors can be explained by the following circumstances.

For a given incoming mode the azimuth spread of trajectories of wave propagation over directions is relatively small: $\Delta\varphi_{\rm eff} \ll 1$. The value of $\Delta\varphi_{\rm eff}$ is estimated as $\Delta\varphi_{\rm eff} \sim \vartheta_0$ at $L < l\vartheta_0$ and $\Delta\varphi_{\rm eff} \sim \zeta_L$ at $L > l\vartheta_0$. The four-fold integration over the azimuth variables [see Eq. (5)] can be presented as the three-fold integration with respect to the differential azimuth variables ($\Delta\varphi = \varphi_a - \varphi_b$, etc.) and one integration with respect to the cumulative azimuth variable $[\varphi_+ = (\varphi_a + \varphi_b + \varphi_c + \varphi_d)/4]$. Within the small-angle approximation each integral with respect to differential azimuth variable $\Delta\varphi$ is extended to infinite limits (from $-\infty$ to $+\infty$] and gives the contribution proportional to $\Delta\varphi_{\rm eff}$. The result of integration over all differential azimuth variables is already independent of the azimuth variable φ_+. Therefore, integration over φ_+ gives the factor 2π. As a result, the four-fold integration over all azimuth variables turns out to be proportional to $\Delta\varphi_{\rm eff}^3$. With allowance for the form of the propagator $I_{ab}(z|z')$ [see Eqs. (28) and (31)] and the differential cross section (25), the rest of the integrals over the ζ angles and coordinates z and z' give a factor which can be written as $1/\Delta\varphi_{\rm eff}^4$. Thus, one factor $1/\Delta\varphi_{\rm eff}$ remains in the final result.

Physically, this means that the variance of conductance fluctuations can be presented as a sum of partial contributions, each being governed by a set of interfering trajectories lying within a narrow azimuth sector of width $\Delta\varphi_{\rm eff}$. Each partial contribution to $\langle(\delta G)^2\rangle$ is a dimensionless quantity of the order of unity. The number of such partial contributions is proportional to $2\pi/\Delta\varphi_{\rm eff}$ and therefore the conductance variance $\langle(\delta G)^2\rangle$ proves to be of the order of $1/\Delta\varphi_{\rm eff}$.

In all calculations presented above we have assumed that the number of modes $N_{\rm eff}$ contributing to the conductance variance should not be small. In the case of small-angle scattering by large inhomogeneities, the number of modes $N_{\rm eff}$ can be estimated as $N_{\rm eff} \sim N \max\{\vartheta_0^2, \zeta_L^2\} \geqslant A/a^2$, where a is the characteristic size of the inhomogeneities. Thus, we suppose that the width of the waveguide is greater than the size of a single inhomogeneity, $\sqrt{A} > a$. This restriction is compatible with the inequality $\sqrt{A} < l$. The latter is a sufficient condition for a disordered system to be considered as quasi-1D at any length L, including the quasiballistic limit (see, e.g., Refs. [11,38,39]).

VII. CONCLUSIONS

In conclusion, we have developed a theoretical approach to calculating the conductance fluctuations in a quasi-1D system, paying special attention to the subdiffusion length scales. We have presented an analytical result which relates the conductance variance to the inhomogeneity characteristics of the disordered system. The conductance fluctuations in the crossover regime have been shown to depend on the kind of disorder. For point-like centers, $\langle(\delta G)^2\rangle$ grows monotonically with increasing waveguide length L and tends to the UCF value in the diffusive limit. Our calculations within the two-stream version of the discrete-ordinate method coincide with the RMT results [10,21–24] for the weak-localization regime (the sample length is much less than the localization length). For a waveguide with large inhomogeneities, the effect of the conductance fluctuation enhancement has been found in the crossover regime. The conductance variance is governed by the trajectories that are nearly perpendicular to the waveguide axis. The regions of second-order scattering ($L < l\vartheta_0$, where ϑ_0 is the characteristic single-scattering angle) and diffusive transport ($L > l_{\rm tr}$) are separated by an intermediate region where the small-angle multiple scattering dominates. The value of $\langle(\delta G)^2\rangle$ has been shown to peak at $L \sim l\vartheta_0$ and then falls off as

$$\langle(\delta G)^2\rangle \sim (l_{\rm tr}/L)^{\nu},$$

where the value of the exponent ν depends on the specific form of the single-scattering law and lies in range $1/3 < \nu < 1$. The peak value of the conductance variance proves to be proportional to $1/\vartheta_0$, thus exceeding the UCF value at $\vartheta_0 \ll 1$.

The results obtained above bridge the gap between the ballistic and diffusive regimes of wave propagation and present a theoretical groundwork for studies of the sensitivity of conductance fluctuations to the specific features of disorder (e.g., the effect of long-range inhomogeneity correlations on the enhancement of fluctuations).

ACKNOWLEDGMENTS

We thank N. B. Narozhny and V. S. Remizovich for useful discussions and valuable advice.

APPENDIX A

In the quasi-1D geometry, a wave field can be expanded in terms of a complete set of transverse modes of the waveguide. For periodic boundary conditions [40], such an expansion has the form

$$\psi(\mathbf{r}) = \frac{1}{\sqrt{A}} \sum_a \psi_a(z) e^{i\mathbf{q}_a\boldsymbol{\rho}}, \quad (\mathbf{q}_a)_{x,y} = \frac{2\pi}{\sqrt{A}} n_{x,y}, \qquad \text{(A1)}$$

where $\boldsymbol{\rho}$ is the transverse component of vector $\mathbf{r}$, A is the area of the waveguide cross section, and $n_{x,y} = 0, \pm1, \pm2, \ldots$. The wave function $\psi_a(z)$ describes a field in the ath mode. The propagating modes correspond to the values of the transverse momentum $|\mathbf{q}_a| < k_0$.

In propagation through a disordered waveguide the wave incoming in the bth mode can be scattered to the ath outgoing

mode. Transmission coefficient T_{ab} connecting incoming b and outgoing a modes is defined as flux density through the output cross section of the waveguide:

$$T_{ab} = \frac{i}{2k_0}\left(\frac{\partial}{\partial z} - \frac{\partial}{\partial z'}\right)\psi_{ab}(z')\psi^*_{ab}(z)\Big|_{z'=z=L}, \quad \text{(A2)}$$

where ψ_{ab} describes the wave field in the ath mode induced by the incident wave in the bth mode. The average coefficient $\langle T_{ab}\rangle$ can be expressed in terms of the ensemble-average second moment $\langle\psi_{ab}(z)\psi^*_{ab}(z')\rangle$ of a wave field and is governed by the sum of ladder diagrams [8].

We define the ladder propagator as

$$\Gamma_{ab}(z,z') = \langle G_{ab}(z,z')G^*_{ab}(z,z')\rangle, \quad \text{(A3)}$$

where $G_{ab}(z,z')$ is the matrix element of the retarded Green function [40].

Under periodic boundary conditions the ensemble-average Green function can be written in the form

$$\langle G_{ab}(z,z')\rangle = G_a(z-z')\delta_{\mathbf{q}_a,\mathbf{q}_b},$$
$$G_a(z-z') = \frac{1}{2i|k_{az}|}\exp\left[\left(i|k_{az}| - \frac{k_0 n\sigma_{\rm tot}}{2|k_{az}|}\right)|z-z'|\right], \quad \text{(A4)}$$

where $k^2_{az} = k^2_0 - \mathbf{q}^2_a$, $\sigma_{\rm tot} = \sigma + \sigma_{\rm a}$ is the total cross section of interaction, σ and $\sigma_{\rm a}$ are the cross sections of elastic scattering and absorption, respectively, and n is the number of scattering centers per unit volume.

The ensemble-average wave field $\langle\psi_{ab}(z)\rangle$ is given by

$$\langle\psi_{ab}(z)\rangle = 2i\sqrt{k_0|k_{bz}|}\langle G_{ab}(z,z'=0)\rangle \quad \text{(A5)}$$

and describes the nonscattered (reduced) incident wave. The field $\langle\psi_{ab}(z)\rangle$ is normalized to unit z component of the incident flux.

The propagator Γ_{ab} obeys the Bethe–Salpeter equation which, in the ladder approximation, is reduced to the ordinary transport equation (see, e.g., Refs. [27,41]). Diagrammatically, this equation is illustrated in Fig. 6. In particular, the first term of the ladder series is proportional to the product of the ensemble-average Green functions and describes the nonscattered incident waves. The second term corresponds to a single scattering and can be written as [see Fig. 6(b)]

$$n\int dz_s G_a(z-z_s)G^*_c(z_1-z_s)\frac{(4\pi)^2}{A}f_{ab}f^*_{cd} \times G_b(z_s-z')G^*_d(z_s-z'_1)\delta_{\mathbf{q}_a-\mathbf{q}_c,\mathbf{q}_b-\mathbf{q}_d}, \quad \text{(A6)}$$

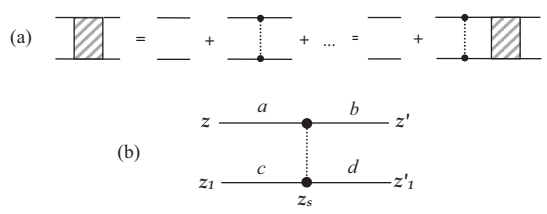

FIG. 6. (a) Diagram series for a ladder propagator. Solid lines denote the average Green function or its complex conjugate. Dotted lines connect identical scatterers. (b) Diagram corresponding to a single-scattering event.

where f_{ab} is the amplitude of scattering from the bth mode to the ath mode. According to definition (A3), this term appears in the transport equation at $\mathbf{q}_a = \mathbf{q}_c$, $\mathbf{q}_b = \mathbf{q}_d$ and $z = z_1, z' = z'_1$. As a result, the transport equation takes the form

$$\Gamma_{ab}(z,z') = |G_a(z-z')|^2\delta_{\mathbf{q}_a,\mathbf{q}_b} + \int dz''\frac{(4\pi)^2}{A} \times \sum_c |G_a(z-z'')|^2\sigma_{ac}\Gamma_{cb}(z'',z'), \quad \text{(A7)}$$

where $\sigma_{ac} = n|f_{ac}|^2$.

For the great number of propagating modes, summation over modes can be replaced by integration over directions of wave propagation [see Eq. (2)]. In this case, it is convenient to go from propagator Γ_{ab} to intensity propagator I_{ab} with the relation

$$I_{ab}(z|z') = 4|k_{az}k_{bz}|\frac{k^2_0 A}{(2\pi)^2}\Gamma_{ab}(z,z'), \quad \text{(A8)}$$

where the quantity $I_{ab}(z|z') \equiv I(z,\mathbf{\Omega}_a|z',\mathbf{\Omega}_b)$ describes the average intensity in the disordered system from a source emitting waves in direction $\mathbf{\Omega}_b$ at depth z'. The ensemble-average transmission coefficient is related to $I_{ab}(z|z')$ by Eq. (3).

As applied to the intensity propagators, the rule of "connection" of two ladder diagrams takes the form

$$\sum_c I_{ac}(z|z'')I_{cb}(z''|z') = \frac{k^2_0 A}{(2\pi)^2}\int d\mathbf{\Omega}_c|\mu_c|I_{ac}(z|z'')I_{cb}(z''|z') = \frac{k^2_0 A}{(2\pi)^2}I_{ab}(z|z'). \quad \text{(A9)}$$

With allowance for Eq. (A8), Eq. (A7) can be rewritten as the ordinary transport equation in the integral form:

$$I_{ab}(z|z') = I^{(0)}_{ab}(z|z') + \frac{1}{|\mu_a|}\int_0^L dz''\exp\left\{-\frac{n\sigma_{\rm tot}(z-z'')}{\mu_a}\right\} \times \eta\left(\frac{z-z''}{\mu_a}\right)\int d\mathbf{\Omega}_c\sigma_{ac}I_{cb}(z''|z'), \quad \text{(A10)}$$

where $\eta(x)$ is the Heaviside step function, and $I^{(0)}_{ab}(z|z')$ is the nonscattered intensity,

$$I^{(0)}_{ab}(z|z') = \frac{1}{|\mu_a|}\delta(\mathbf{\Omega}_a - \mathbf{\Omega}_b)\exp\left\{-\frac{n\sigma_{\rm tot}(z-z')}{\mu_a}\right\} \times \eta\left(\frac{z-z'}{\mu_a}\right). \quad \text{(A11)}$$

By substituting Eq. (A11) into the integral term in the right-hand side of Eq. (A10), we obtain the single-scattering contribution to the intensity propagator. Continuing the iterative procedure in Eq. (A10), we can derive all terms of expansion of the intensity propagator in the orders of scattering.

Acting on Eq. (A10) by the operator $\mu_a(\partial/\partial z) + n\sigma_{\rm tot}$, we bring the transport equation into the standard integro-differential form [see Eq. (4)].

APPENDIX B

The variance of conductance fluctuations

$$\langle(\delta G)^2\rangle = \sum_{a\,b\,c\,d} \langle \delta T_{ab} \delta T_{cd}\rangle \tag{B1}$$

can be expressed in terms of the ensemble-average fourth moment of a wave field and represented as an expansion in orders of interference between ladder graphs. Each interference event between the ladders contains the Hikami vertex [26] (see also Refs. [5,7,8]).

First we consider the diagram that involves a single Hikami vertex with four attached ladder propagators [see Fig. 7(a)]. This diagram can be thought of as a building block appearing in diagrams shown in Fig. 1. The contribution from the "empty" Hikami box can be calculated as follows: For $k_0 l \gg 1$, the product of the Green functions appearing in the empty box is nonzero as long as the phases of the Green functions compensate for each other [28]. With allowance for the transverse-momentum conservation [see Eq. (A6)] in the ladder propagators attached to the box, the Green functions entering into the box must be identical in mode:

$$G_a(z-z_2)G_a^*(z_2-z')G_a(z'-z_1)G_a^*(z_1-z). \tag{B2}$$

The phases of the Green functions entering into Eq. (B2) compensate for each other provided that points z, z', z_1, z_2 are ordered in the same manner as shown in the first two graphs of Fig. 7(b). The alignment of these points in the product of the Green functions can be found by evaluating the corresponding integral with the stationary-phase method [27]. Points z, z', z_1, z_2 are grouped in pairs as (z, z') and (z_1, z_2). The mutual arrangement of these pairs as well as the point positions in each pair can be arbitrary. If point z' and pair (z_1, z_2) lie on opposite sides with respect to z, the difference $|z_{1,2} - z'|$ can be presented as $|z_{1,2} - z'| = |z_{1,2} - z| + |z - z'|$. Then the Green function $G_a(z' - z_1)$ is equal to

$$G_a(z'-z_1) = 2i|k_{az}|G_a(z-z_1)G_a(z'-z). \tag{B3}$$

A similar equality can also be written for $G_a^*(z_2 - z')$. In this case Eq. (B2) takes the following form:

$$4k_{az}^2|G_a(z-z')|^2|G_a(z_1-z)|^2|G_a(z_2-z)|^2. \tag{B4}$$

If point z' lies between point z and pair (z_1,z_2), the arguments z and z' in Eq. (B4) should be interchanged.

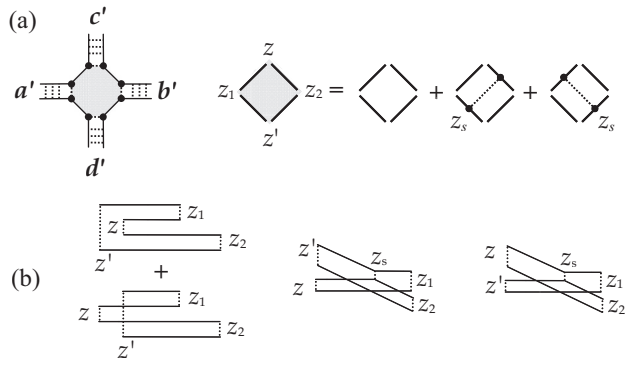

FIG. 7. (a) Hikami vertex with four attached ladder propagators. (b) Arrangement of scattering events in the Hikami vertex.

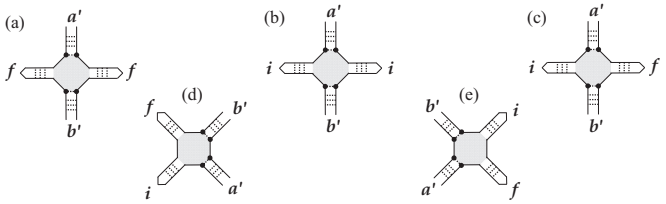

FIG. 8. Single-Hikami-vertex blocks appearing in the diagrams for the conductance variance. Converging solid lines to a point denotes summation over all outgoing (or incoming) modes.

Taking advantage of the transport equation [see Eqs. (A7) and (A10)] and rule (A9), we can attach the propagators to the empty box to give

$$\left(\frac{\pi}{N}\right)^3 \int dz \iint d\mathbf{\Omega}_a d\mathbf{\Omega}_b \sigma_{ab} I^{\rm sc}_{a'a}(\cdots|z)\, I^{\rm sc}_{b'a}(\cdots|z) \times \left[I^{\rm sc}_{bc'}(z|\cdots)\, I^{\rm sc}_{ad'}(z|\cdots) + I^{\rm sc}_{ac'}(z|\cdots)\, I^{\rm sc}_{bd'}(z|\cdots)\right], \tag{B5}$$

where $N = k_0^2 A/(4\pi)$ is the number of modes, and a "scattered" propagator is defined as $I^{\rm sc} = I - I^{(0)}$.

The contribution from the diagrams involving the Hikami box with one extra scattering can be calculated in a similar way. The mutual arrangement of points z, z', z_1, z_2, and z_s that results in compensating the Green function phases are depicted in the second two graphs of Fig. 7(b). In one case the product of the Green functions appearing in the Hikami box takes the form

$$4|k_{az}k_{bz}|\frac{(4\pi)^2\sigma_{ab}}{A}|G_a(z-z_s)|^2|G_b(z'-z_s)|^2 \times |G_a(z_s-z_1)|^2|G_b(z_s-z_2)|^2. \tag{B6}$$

For the other diagram with one extra scattering, the product of the Green functions is obtained from Eq. (B6) by interchanging z_1 and z_2. Then, attaching the propagators to the Hikami box, we find

$$-\left(\frac{\pi}{N}\right)^3 \int dz \iint d\mathbf{\Omega}_a d\mathbf{\Omega}_b \sigma_{ab} \left[I^{\rm sc}_{a'a}(\cdots|z) I^{\rm sc}_{b'b}(\cdots|z) + I^{\rm sc}_{a'b}(\cdots|z) I^{\rm sc}_{b'a}(\cdots|z)\right] I^{\rm sc}_{ac'}(z|\cdots) I^{\rm sc}_{bd'}(z|\cdots). \tag{B7}$$

By combining Eqs. (B5) and (B7), we arrive at the following expression for the single-Hikami-vertex contribution:

$$\left(\frac{\pi}{N}\right)^3 \int dz \iint d\mathbf{\Omega}_a d\mathbf{\Omega}_b \sigma_{ab} \left[I^{\rm sc}_{a'a}(\cdots|z) - I^{\rm sc}_{a'b}(\cdots|z)\right] \times \left[I^{\rm sc}_{b'a}(\cdots|z) - I^{\rm sc}_{b'b}(\cdots|z)\right] I^{\rm sc}_{ac'}(z|\cdots) I^{\rm sc}_{bd'}(z|\cdots). \tag{B8}$$

The propagators entering into Eq. (B8) can also be "read" in the reverse order [i.e., propagators $I^{\rm sc}_{a'a}(\ldots|z)$ and $I^{\rm sc}_{bd'}(z|\ldots)$ are replaced by $I^{\rm sc}_{aa'}(z|\ldots)$ and $I^{\rm sc}_{d'b}(\ldots|z)$, respectively]. In addition, Eq. (B8) can be rewritten in the form that is obtained by interchanging pairs a', b' and c', d'. All these representations are equivalent to each other and applied below to evaluating the second-order diagrams in the Hikami vertex.

The different single-Hikami-vertex blocks appearing in the diagrammatic rendering of the conductance variance are illustrated in Fig. 8. The incoming and outgoing propagators are shown as the ladder graphs with the solid lines converging to a point. This corresponds to summation over all incoming

(or outgoing) modes in the source (or in the receiver). The incoming and outgoing propagators are thought of as incorporating an arbitrary number of scattering events (including no one event). The diagrams with one or two "nonscattered" incoming (or outgoing) propagators are calculated much as it has been done above with the only difference being that one or two points involved in the Hikami box turn out to be coincident with position z_i (or z_f) of the input (or output) waveguide cross section, and not with the position of the first (last) scattering event in the attached propagator.

The first diagram of Fig. 1 consists of the blocks shown in Figs. 8(a) and 8(b). The contributions of these blocks are obtained from Eq. (B8) by summation over modes a' and b'. In particular, the diagram in Fig. 8(a) gives

$$\frac{\pi}{N}\int dz \iint d\mathbf{\Omega}_a d\mathbf{\Omega}_b \sigma_{ab}\left[I_a^f(z)-I_b^f(z)\right]^2 \times I^{\mathrm{sc}}_{aa'}(z|\cdots)I^{\mathrm{sc}}_{bb'}(z|\cdots), \tag{B9}$$

where

$$I_a^f(z)=\frac{\pi}{N}\sum_b I_{ba}(z_f|z). \tag{B10}$$

A similar expression can be written for the diagram 8(b) [the difference between the incoming propagators $I_a^i(z)-I_b^i(z)$ should be substituted for $I_a^f(z)-I_b^f(z)$ into Eq. (B9)]. By combining the expressions for diagrams 8(a) and 8(b), we obtain the following contribution to the conductance variance:

$$\langle(\delta G)^2\rangle = \iint dzdz' \iiiint d\mathbf{\Omega}_a d\mathbf{\Omega}_b d\mathbf{\Omega}_c d\mathbf{\Omega}_d \sigma_{ab}\sigma_{cd} \times\left[I_a^f(z)-I_b^f(z)\right]^2 I^{(\geqslant 2)}_{ac}(z|z')I^{(\geqslant 2)}_{bd}(z|z') \times\left[I_c^i(z')-I_d^i(z')\right]^2, \tag{B11}$$

where the internal propagators are supposed to include no less than two scattering events [regarding low-order-scattering terms in $I_{ac}(z|z')I_{bd}(z|z')$; see below].

In the presence of time-reversal symmetry, Eq. (B11) should be supplemented by the contribution of the diagram which is obtained from that discussed above by interchanging the initial z_i and final z_f points in one pair of conjugated wave fields. This latter diagram consists of two identical blocks similar to the diagram in Fig. 8(c) and is responsible for the second term of Eq. (5). The corresponding contribution to the conductance variance differs from Eq. (B11) only by substitution of multipliers $[I_a^f(z)-I_b^f(z)][I^i_{-a}(z)-I^i_{-b}(z)]$ and $[I^f_{-c}(z')-I^f_{-d}(z')][I_c^i(z')-I_d^i(z')]$ for $[I_a^f(z)-I_b^f(z)]^2$ and $[I_c^i(z')-I_d^i(z')]^2$, respectively. Propagators $I^{i,f}_{-a}$ differ from $I^{i,f}_a$ by substitution of $-\mathbf{q}_a$ for $\mathbf{q}_a$ (or $-\mathbf{\Omega}_a$ for $\mathbf{\Omega}_a$). The reciprocity relation $I_{ab}(z|z')=I_{-b-a}(z'|z)$ should also be taken into account.

The second diagram of Fig. 1 can be represented as combination of the two single-Hikami-vertex blocks depicted in Figs. 8(d) and 8(e). According to the rules derived above, the diagram in Fig. 8(d) gives

$$\frac{\pi}{N}\int dz \iint d\mathbf{\Omega}_a d\mathbf{\Omega}_b \sigma_{ab}\left[I_a^f(z)-I_b^f(z)\right] \times\left[I^{\mathrm{sc}}_{-a-a'}(z|\cdots)-I^{\mathrm{sc}}_{-b-a'}(z|\cdots)\right]I^{\mathrm{sc}}_{ab'}(z|\cdots)I_b^i(z). \tag{B12}$$

The contribution from the diagram in Fig. 8(e) can be written in a similar way by interchanging the corresponding propagators. Combining these results we obtain

$$\langle(\delta G)^2\rangle = \iint dzdz' \iiiint d\mathbf{\Omega}_a d\mathbf{\Omega}_b d\mathbf{\Omega}_c d\mathbf{\Omega}_d \sigma_{ab}\sigma_{cd} \times\left[I_a^f(z)-I_b^f(z)\right]I_b^i(z)\left[I^{(\geqslant 2)}_{ac}(z|z')-I^{(\geqslant 2)}_{ad}(z|z')\right] \times\left[I^{(\geqslant 2)}_{-a-c}(z|z')-I^{(\geqslant 2)}_{-b-c}(z|z')\right]I_d^i(z')\left[I_c^f(z')-I_d^f(z')\right]. \tag{B13}$$

The second diagram shown in Fig. 1 is supposed to include two contributions which are related to each other by complex conjugation. The conjugated contribution can be derived similarly to Eq. (B13). To symmetrize the final result, we interchange the propagators attached to the opposite ends of the Hikami vertex. Then multipliers $[I_a^f(z)-I_b^f(z)]I_b^i(z)$ and $[I_c^f(z')-I_d^f(z')]I_d^i(z')$ are replaced by $[I^i_{-a}(z)-I^i_{-b}(z)]I^f_{-b}(z)$ and $[I^i_{-c}(z')-I^i_{-d}(z')]I^f_{-d}(z')$, respectively.

The contribution from the time-reversed counterpart of the second diagram shown in Fig. 1 differs from Eq. (B13) by interchanging the incoming and outgoing propagators in one of the products [either $[I_a^f(z)-I_b^f(z)]I_b^i(z)$ or $[I_c^f(z')-I_d^f(z')]I_d^i(z')$ should be replaced by $[I^i_{-a}(z)-I^i_{-b}(z)]I^f_{-b}(z)$ or $[I^i_{-c}(z')-I^i_{-d}(z')]I^f_{-d}(z')$, respectively]. Combining these four contributions we obtain the third term in Eq. (5).

The diagrams shown in Fig. 1 can be evaluated by combining two single-Hikami-vertex blocks provided that each internal propagator includes no less than two scattering events. Otherwise, these diagrams cannot be presented as combination of two blocks. The "irreducible" diagrams can be exemplified by the diagram with two empty Hikami boxes and one nonscattered internal propagator [see Fig. 9(a)]. The other internal propagator is supposed to include no less than two scattering events. In this case, the central part of the diagram contains six Green functions. Due to the transverse momentum conservation, these Green functions relate to identical modes. The phases of the Green functions compensate for each other provided that the scattering events are ordered in the same manner as shown in Fig. 9(b). By using relations similar to Eq. (B3) and attaching the ladders to the central part, we obtain the following result:

$$\begin{aligned}\langle(\delta G)^2\rangle = \iint dz_{\ldots}dz_{\ldots} \iiiint d\mathbf{\Omega}_a d\mathbf{\Omega}_b d\mathbf{\Omega}_c d\mathbf{\Omega}_d \sigma_{ab}\sigma_{cd}\Big\{&\left[I_a^f(z)\right]^2 I^{(0)}_{ac}(z|z')I_{bd}(z|z')\left[I_c^i(z')\right]^2 \\ &+ I_a^f(z_1)I_b^i(z_1)I^{(0)}_{ad}(z_1|z)I^{sc}_{-a-c}(z_1|z)I_d^f(z)I_d^i(z) + I_b^f(z)I_b^i(z)I^{sc}_{ac}(z|z_2)I^{(0)}_{-b-c}(z|z_2)I_c^f(z_2)I_d^i(z_2) \\ &+ I_a^f(z_1)I_b^i(z_1)\left[I^{(0)}_{ac}(z_1|z_2)I^{(\geqslant 2)}_{-a-c}(z_1|z_2)+I^{(\geqslant 2)}_{ac}(z_1|z_2)I^{(0)}_{-a-c}(z_1|z_2)\right]I_c^f(z_2)I_d^i(z_2)\Big\} \\ &+ \int dz \iint d\mathbf{\Omega}_a d\mathbf{\Omega}_b \sigma_{ab}\left[I_b^f(z)\right]^2 I^{sc}_{ab}(z|z)\left[I_b^i(z)\right]^2.\end{aligned} \tag{B14}$$

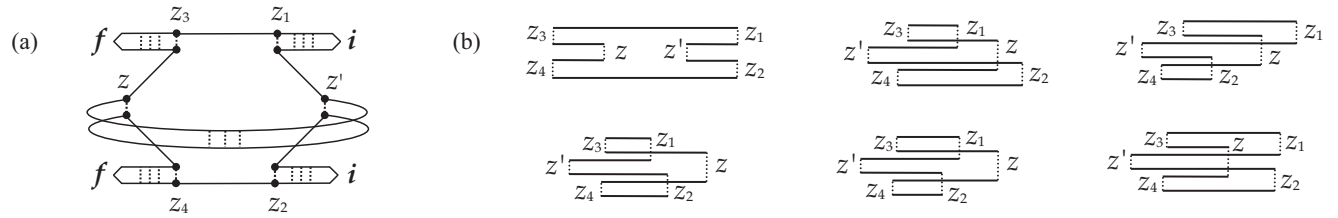

FIG. 9. (a) Diagram with two empty Hikami boxes and one empty internal propagator. (b) Variants of the mutual arrangement of scattering events.

The terms appearing in the first three lines of Eq. (B14) can be considered as low-order-scattering contributions from the both diagrams depicted in Fig. 1. This terms can be combined with the "multiple-scattering" contributions to $\langle(\delta G)^2\rangle$, to result in partial removing the restrictions on the number of scattering events included in the internal propagators.

The last alignment of scattering events shown in Fig. 9(b) is responsible for the "local" term appearing in the last line of Eq. (B14). This contribution includes only one internal propagator that describes propagation of waves along a loop trajectory. Such local terms appear also in evaluating diagrams which include an additional single-scattering event either in the Hikami boxes or in the internal propagator (previously supposed to be empty). All such contributions are combined to give the corresponding local term entering into Eq. (5).

To remove finally the restrictions on the number of scattering events in the internal propagators, the results obtained above should be supplemented by the contribution from low-order scattering graphs between incoming and outgoing propagators (these diagrams are exemplified in Fig. 10). All contributions from single-scattering events between the propagators cancel each other (see, e.g., Ref. [5]). Depending on the mutual arrangement of the low-order scattering events along the z axis, these diagrams contribute to one or another terms of Eq. (5) [the "mushroom-shaped" graphs shown in Fig. 10 contribute only to the third term of Eq. (5); these graphs are originated from the second diagram of Fig. 1].

As an example, we present the result of calculations of the first diagram shown in Fig. 10. There are two different contributions to $\langle(\delta G)^2\rangle$ from this diagram. One term contains the factor σ_{ab}. The other corresponds to the waves propagating towards each other and gives the product of the scattering amplitudes of the form $f_{ab}f_{-b-a}$. The sum of these contributions

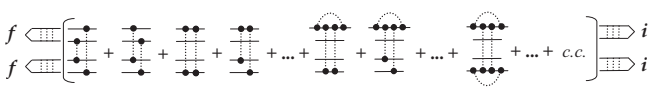

FIG. 10. Examples of diagrams containing low-order scattering between incoming and outgoing propagators. These diagrams should also be supplemented by their conjugated counterparts and by the diagrams that differ from those presented by interchanging initial i and final f states in one or two pairs of propagators.

to $\langle(\delta G)^2\rangle$ can be written as

$$\begin{aligned}\langle(\delta G)^2\rangle = &\iint_0^L dz dz' \iiiint d\mathbf{\Omega}_a d\mathbf{\Omega}_b d\mathbf{\Omega}_c d\mathbf{\Omega}_d \\ &\times I^{(0)}_{ac} I^{(0)}_{bd} \{\sigma^2_{ab}\left[\left(I^f_a\right)^2\left(I^i_d\right)^2 + \left(I^f_b\right)^2\left(I^i_c\right)^2\right] \\ &+ \left(f_{ab}f_{-b-a}\right)^2\left[I^f_a I^i_{-a} I^f_{-d} I^i_d + I^f_b I^i_{-b} I^f_{-c} I^i_c\right]\} \\ &+ \int_0^L dz \iint d\mathbf{\Omega}_a d\mathbf{\Omega}_b \\ &\times \left\{\sigma_{ab} I^{(1)}_{ab}\left[\left(I^f_a I^i_b\right)^2 + \left(I^f_{-b} I^i_{-a}\right)^2\right]\right. \\ &\left.+ f_{ab}f_{-b-a}\tilde{I}^{(1)}_{ab}\left[I^f_a I^i_b I^f_{-b} I^i_{-a} + I^f_{-b} I^i_{-a} I^f_a I^i_b\right]\right\},\end{aligned} \tag{B15}$$

where $\tilde{I}^{(1)}_{ab}$ is obtained from $I^{(1)}_{ab}$ by substitution of $f_{ab}f_{-b-a}$ for σ_{ab}. Equation (B15) contributes to the first two terms as well as to the local term of Eq. (5).

Taking into account all diagrams that include low-order-scattering events between incoming and outgoing propagators, we gather step by step low-order-scattering contributions to the internal propagators appearing in Eq. (5) and remove the restrictions imposed on the number of scattering events in Eqs. (B11) and (B13).

APPENDIX C

According to the method of discrete ordinates [27,29], a solution of the transport equation (4) is sought on the grid of the angular variable values μ_k, $k = 1, \ldots, K$. Within such an approach, all integrals over directions are replaced by the corresponding sums and the transport equation transforms to a set of K coupled differential equations. The simplest version of the discrete-ordinate method can be implemented at $K = 2$. This corresponds to the "two-stream" approximation.

Within the two-stream approximation Eq. (4) transforms to a set of two ordinary differential equations for the forward and backward fluxes [27,29]. For point-like scattering centers, these equations take the form

$$\begin{aligned}\left(\mu_0\frac{\partial}{\partial z} + n\sigma_{\rm tot}\right) I_+ &= \frac{n\sigma}{2}\left(I_+ + I_-\right), \\ \left(-\mu_0\frac{\partial}{\partial z} + n\sigma_{\rm tot}\right) I_- &= \frac{n\sigma}{2}\left(I_- + I_+\right),\end{aligned} \tag{C1}$$

where $I_\pm(z) = I(z, \Omega_z = \pm\mu_0)$, and $\pm\mu_0$ are the discrete ordinates.

The internal propagators $I_{\pm,+}(z|z')$ and $I_{\pm,-}(z|z')$ appearing in Eq. (17) are the solutions to these equations for a source placed at z' and emitting waves in directions $+\mu_0$ and $-\mu_0$ (see the second sign in the subscripts). In the case of a nonabsorbing medium, the propagators $I_{\pm,+}(z|z')$ can be written as

$$I_{++}(z|z') = \frac{1}{2\pi\mu_0\,(s_L+1)}\begin{cases} s(s_L-s'), & z<z' \\ (s'+1)(s_L-s+1), & z>z', \end{cases} \tag{C2}$$

$$I_{-+}(z|z') = \frac{1}{2\pi\mu_0\,(s_L+1)}\begin{cases} (s+1)(s_L-s'), & z<z' \\ (s_L-s)(s'+1), & z>z', \end{cases} \tag{C3}$$

where $s_L = L/(2\mu_0 l)$, $s = z/(2\mu_0 l)$, and $l = (n\sigma)^{-1}$ is the mean-free path. For a source emitting waves in direction $-\mu_0$, the corresponding solution is expressed in terms of Eqs. (C2) and (C3) as follows:

$$I_{--}(z|z') = I_{++}(z'|z), \quad I_{+-}(z|z') = I_{-+}(L-z|L-z'). \tag{C4}$$

The incoming and outgoing propagators are described by the relations

$$\begin{aligned} I^i_{\pm}(z) &= 2\pi\mu_0 I_{\pm+}\,(z|z_i=0)\,, \\ I^f_{\pm}(z) &= 2\pi\mu_0 \begin{cases} I_{+\pm}\,(z_f=L|z) & \text{for transmission} \\ I_{-\pm}\,(z_f=0|z) & \text{for reflection.} \end{cases} \end{aligned} \tag{C5}$$

In the presence of absorption, Eqs. (C2) and (C3) are replaced by

$$I_{++}(z|z') = \frac{1}{2\pi\mu_0 \sinh(\gamma)\sinh(\xi_L+\gamma)} \times \begin{cases} \sinh(\xi)\sinh(\xi_L-\xi'), & z<z' \\ \sinh(\xi'+\gamma)\sinh(\xi_L-\xi+\gamma), & z>z', \end{cases} \tag{C6}$$

$$I_{-+}(z|z') = \frac{1}{2\pi\mu_0 \sinh(\gamma)\sinh(\xi_L+\gamma)} \times \begin{cases} \sinh(\xi+\gamma)\sinh(\xi_L-\xi'), & z<z' \\ \sinh(\xi'+\gamma)\sinh(\xi_L-\xi), & z>z', \end{cases} \tag{C7}$$

where $\xi = s\sinh(\gamma)$, $\xi_L = s_L\sinh(\gamma)$, and $\sinh(\gamma) = 2\sqrt{l(l+l_a)}/l_a$, $l_a = (n\sigma_a)^{-1}$ is the absorption length. Relations (C4) and (C5) remain unchanged.

The average conductance and reflectance can be expressed in terms of the propagator values at the output and input boundaries:

$$\begin{aligned} \langle G\rangle &= 2\pi\mu_0 N I_{++}(z_f=L|z_i=0), \\ \langle R\rangle &= 2\pi\mu_0 N I_{-+}(z_f=0|z_i=0), \end{aligned} \tag{C8}$$

where N is the total number of modes. For samples with no absorption, from Eqs. (C2), (C3), and (C8), it follows that

$$\langle G\rangle = N\frac{1}{s_L+1}, \quad \langle R\rangle = N\frac{s_L}{s_L+1}. \tag{C9}$$

In the presence of absorption, Eqs. (C6)–(C8) result in

$$\langle G\rangle = N\frac{\sinh(\gamma)}{\sinh(\xi_L+\gamma)}, \quad \langle R\rangle = N\frac{\sinh(\xi_L)}{\sinh(\xi_L+\gamma)}. \tag{C10}$$

With allowance for the rule of correspondence [30], Eqs. (C9) and (C10) are in agreement with RMT results [10,21,23,24]. Relations (C9) coincide with those of Refs. [21,23,24]. Relations (C10) transforms to the corresponding results of Ref. [10] in the diffusive limit (large lengths, $L \gg l$, and weak absorption, $l_a \gg l$).

[1] B. L. Altshuler, JETP Lett. **41**, 648 (1985); P. A. Lee and A. D. Stone, Phys. Rev. Lett. **55**, 1622 (1985).
[2] P. A. Lee, A. D. Stone, and H. Fukuyama, Phys. Rev. B **35**, 1039 (1987).
[3] F. Scheffold and G. Maret, Phys. Rev. Lett. **81**, 5800 (1998).
[4] P. Sebbah, B. Hu, A. Z. Genack, R. Pnini, and B. Shapiro, Phys. Rev. Lett. **88**, 123901 (2002); A. A. Chabanov, N. P. Tregoures, B. A. van Tiggelen, and A. Z. Genack, *ibid.* **92**, 173901 (2004).
[5] C. L. Kane, R. A. Serota, and P. A. Lee, Phys. Rev. B **37**, 6701 (1988).
[6] P. A. Mello, E. Akkermans, and B. Shapiro, Phys. Rev. Lett. **61**, 459 (1988).
[7] S. Feng, C. Kane, P. A. Lee, and A. D. Stone, Phys. Rev. Lett. **61**, 834 (1988).
[8] M. C. W. van Rossum, Th. M. Nieuwenhuizen, and R. Vlaming, Phys. Rev. E **51**, 6158 (1995); M. C. W. van Rossum and Th. M. Nieuwenhuizen, Rev. Mod. Phys. **71**, 313 (1999).
[9] A. V. Tartakovski, Phys. Rev. B **52**, 2704 (1995).
[10] P. W. Brouwer, Phys. Rev. B **57**, 10526 (1998).
[11] P. Mohanty and R. A. Webb, Phys. Rev. Lett. **88**, 146601 (2002).
[12] T. Ludwig, Ya. M. Blanter, and A. D. Mirlin, Phys. Rev. B **70**, 235315 (2004).
[13] K. Kechedzhi, O. Kashuba, and V. I. Falko, Phys. Rev. B **77**, 193403 (2008); M. Yu. Kharitonov and K. B. Efetov, *ibid.* **78**, 033404 (2008).
[14] N. Cherroret, A. Pena, A. A. Chabanov, and S. E. Skipetrov, Phys. Rev. B **80**, 045118 (2009).
[15] A. Rycerz, J. Tworzydlo, and C. W. J. Beenakker, Europhys. Lett. **79**, 57003 (2007).
[16] E. Rossi, J. H. Bardarson, M. S. Fuhrer, and S. Das Sarma, Phys. Rev. Lett. **109**, 096801 (2012).
[17] Y. Takagaki and K. H. Ploog, Phys. Rev. B **63**, 125311 (2001).
[18] T. Ando, J. Phys. Soc. Jpn. **73**, 1895 (2004).
[19] T. Markussen, R. Rurali, A.-P. Jauho, and M. Brandbyge, Phys. Rev. Lett. **99**, 076803 (2007).

[20] F. Iori, S. Ossicini, and R. Rurali, J. Appl. Phys. **116**, 074303 (2014).
[21] P. A. Mello, Phys. Rev. Lett. **60**, 1089 (1988); P. A. Mello and A. D. Stone, Phys. Rev. B **44**, 3559 (1991).
[22] T. Sh. Misirpashaev and C. W. J. Beenakker, JETP Lett. **64**, 319 (1996).
[23] A. Garcia-Martin, F. Scheffold, M. Nieto-Vesperinas, and J. J. Saenz, Phys. Rev. Lett. **88**, 143901 (2002).
[24] L. S. Froufe-Perez, A. Garcia-Martin, G. Cwilich, and J. J. Saenz, Phys. A (Amsterdam, Neth.) **386**, 625 (2007).
[25] P. A. Mello and B. Shapiro, Phys. Rev. B **37**, 5860 (1988).
[26] S. Hikami, Phys. Rev. B **24**, 2671 (1981).
[27] A. Ishimaru, *Wave Propagation and Scattering in Random Media*, IEEE Press Series on Electromagnetic Wave Theory (Wiley, New York, 1999).
[28] D. B. Rogozkin and M. Y. Cherkasov, Phys. Rev. B **51**, 12256 (1995).
[29] S. Chandrasekhar, *Radiative Transfer* (Dover Publications, New York, 1960).
[30] For given L/l our results coincide with the RMT calculations [10,21–24] provided that we put absorption length $l_a = 2l_a^{\mathrm{RMT}}$, and discrete ordinate μ_0 is chosen to be equal to $1/2$ which corresponds to the isotropy hypothesis underlying RMT.
[31] R. G. Newton, *Scattering Theory of Waves and Particles* (Dover, New York, 2002).
[32] M. V. Berry and I. C. Percival, Opt. Acta **33**, 577 (1986); A. Pearson and R. W. Anderson, Phys. Rev. B **48**, 5865 (1993); M. Hunter, V. Backman, G. Popescu, M. Kalashnikov, C. W. Boone, A. Wax, V. Gopal, K. Badizadegan, G. D. Stoner, and M. S. Feld, Phys. Rev. Lett. **97**, 138102 (2006); C. J. R. Sheppard, Opt. Lett. **32**, 142 (2007).
[33] S. V. Maleyev, Phys. Rev. B **52**, 13163 (1995).
[34] L. I. Glazman and M. Jonson, Phys. Rev. B **44**, 3810 (1991).
[35] V. S. Remizovich, Sov. Phys. JETP **60**, 290 (1984).
[36] E. E. Gorodnichev and D. B. Rogozkin, JETP **24**, 112 (1995).
[37] A. I. Kuzovlev and V. S. Remizovich, Radiophys. Quantum Electron. (Engl. Transl.) **33**, 778 (1990); Phys. Rev. A **48**, 465 (1993).
[38] O. N. Dorokhov, Sov. Phys. JETP **58**, 606 (1983).
[39] H. Tamura and T. Ando, Phys. Rev. B **44**, 1792 (1991).
[40] D. S. Fisher and P. A. Lee, Phys. Rev. B **23**, 6851 (1981).
[41] U. Frisch, in *Probabilistic Methods in Applied Mathematics*, edited by A. T. Barucha-Reid (Academic Press, New York, 1968), Vol. 1, pp. 75–198.